

The Faint End of the Galaxy Luminosity Function in Moderate Redshift Clusters

Gillian Wilson,^{1,4} Ian Smail,¹ Richard S. Ellis² & Warrick J. Couch³

1) *Department of Physics, University of Durham, South Rd., Durham DH1 3LE.*

2) *Institute of Astronomy, Madingley Rd, Cambridge CB3 0HA.*

3) *School of Physics, University of NSW, Sydney 2052, NSW Australia.*

4) *Canadian Institute for Theoretical Astrophysics, University of Toronto, 60 St. George St., Toronto, Canada M5S 1A7.*

DRAFT: 1 October 2018

ABSTRACT

We present deep two-colour photometry of two rich clusters at $z = 0.18$, A665 and A1689. We use these data to construct number counts as a function of magnitude in the two fields. By combining these counts with similar observations from a large area field survey we subtract the field contamination statistically to produce luminosity functions for the two clusters. Great care has been taken to achieve agreement between the photometry of these two samples. The cluster data are complete to a limiting magnitude of $I = 22.5$ or an absolute magnitude in the cluster of $I = -18.0$ ($M^* + 5$). The luminosity functions of both clusters are well described by a Gaussian function for the bright galaxies, combined with a Schechter function at the faint end, similar to that required to fit the luminosity function in local clusters. The slope at the faint end of the Schechter function in both clusters is extremely steep in V , $\alpha \sim -2$. A shallower slope is seen to the limit of the I data, indicating that the cluster population is rapidly blueing as we reach fainter. The excellent agreement between the form of the luminosity function in our two distant clusters, as well as agreement with the luminosity function given by Driver et al. (1994) for a single $z = 0.21$ cluster, indicates that this faint blue population is a general constituent of distant clusters. We compare our results with those from studies of local clusters. Depending upon the degree of fading (or disruption) of these faint blue galaxies, we tentatively identify their remnants with the low surface brightness dwarf galaxies which are the dominant population in local clusters. We discuss the possible role of this population as the source of most of the X-ray gas in rich clusters.

Key words: cosmology: observations – clusters: individual: A665, A1689 – galaxy evolution – galaxies: photometry – galaxies: luminosity function.

1 INTRODUCTION

The form of the luminosity function (LF) of galaxies is a critical constraint on models of galaxy formation (Cole et al. 1994). To measure accurately the form of the galaxy luminosity function to faint magnitudes requires the determination of distances to large numbers of faint galaxies. Observationally this is a very expensive procedure to undertake for field galaxies, as the individual distances must be measured spectroscopically. However, by studying a rich cluster where the bulk of the population is at a single distance, the practicalities of LF estimation are optimised. Unfortunately, this advantage comes at a price; rich clusters are regions where

we might expect environmental effects on the form of the luminosity function to have their greatest impact, evidence for which may already exist in the observed morphology-density relationship (Dressler 1980; Whitmore, Gilmore, & Jones 1993). Nevertheless, by studying a number of clusters with a range of properties it may be possible to gauge the effect of the environment on their galaxy populations (itself an interesting issue) and hence determine the likely similarity of field and cluster LFs. It is for this reason that much recent work has been concentrated on rich clusters.

A photographic study of 14 rich clusters by Colless (1987) and another 9 clusters by Lugger (1986) concluded

that all clusters could be fit by a universal LF with $\alpha \sim -1.25$ to $M_V \sim -19^*$. More recent work has come to somewhat different conclusions. Kashikawa et al. (1995) carried out a photometric survey of both morphologically-classified subsamples and the composite LF's of four nearby clusters, including Coma. They found a faint end upturn which led to a rejection of a single Schechter function with $\alpha \sim -1.25$ as an adequate representation of the data; a combination of a Gaussian at the bright end and a Schechter function at the faint end being preferred. A faint end upturn in Coma was originally seen by Abell (1977) and later Metcalfe (1983) (See also Thompson & Gregory (1993), Biviano et al. (1995) and Secker & Harris (1996), all of whom also prefer the combined Gaussian+Schechter function description of the LF). However, we note that Bernstein et al. (1996) found no upturn in their counts in the *core* region of Coma.

In a seminal paper Binggeli, Sandage, & Tammann (1985) published the LF derived from their extensive study of the galaxy population in the Virgo region. The advantage of working in the Virgo cluster is that its relative proximity means that it is possible to reach far down the LF. Using deep plate material they classified the galaxy populations morphologically and then derived luminosity functions for various types. The brighter cluster ellipticals apparently follow a Gaussian distribution, while the faint end of the LF is dominated by a population of dwarf ellipticals which impart a steeply rising faint end slope to the LF ($\alpha \sim -1.35$). Later, Impey, Bothun, & Malin (1988) (see also Bothun, Impey, & Malin 1991) surveyed both Virgo and Fornax for low surface brightness (LSB) objects and found many galaxies missed by Binggeli et al. (1985), steepening α yet further to ~ -1.7 in Virgo (brighter than $M_V \sim -12$). While the breakdown of the LF into its separate morphological constituents was extremely illuminating, this type of study can only be performed for nearby clusters from the ground (although see Smail et al. (1996) for a study of distant clusters using HST) and suffers from uncertain corrections for field contamination.

A general picture is thus emerging of the form of the luminosity function for local clusters. The LF appears to be best described by combining a Gaussian distribution for the bright (giant) galaxies with a Schechter function for the fainter (dwarf) galaxies. The very steep slope of the faint component results in it being the dominant galactic component in the clusters. The evolution of this population is thus critical for understanding, for example, how the blue star forming galaxies seen in the cores of distant ($z \geq 0.2$) Butcher-Oemler clusters (Butcher & Oemler 1984; Oemler 1992) have evolved by the present-day. These galaxies should still populate such regions, although their appearance will depend sensitively upon their subsequent star formation histories. One recently proposed mechanism for transforming them is "galaxy harassment" (Moore et al. 1996). In this model star forming field galaxies falling into the cluster potential have their dark halos stripped, as well as undergoing tidal encounters with cluster galaxies. These processes re-

move the outer baryonic material from the galaxy disk and concentrate its remaining gas in a nuclear starburst. The end product of the process is suggested to be a dwarf spheroidal galaxy. Within the framework of such a model we would expect the dwarf/giant spheroid ratio of the cluster to increase rapidly with cosmic epoch, as increasing numbers of infalling galaxies are transformed into dwarfs.

Another area of research which is sensitive to the form of the faint end of the LF in distant clusters is the source of intracluster gas and its enrichment. Trentham (1994) has suggested that a large fraction of the hot intracluster gas seen in Coma may have originated in dwarf galaxies which, after an initial burst of star formation, expelled their gas into the cluster potential and subsequently faded to become the LSB dwarf galaxy population observed today (or disrupted completely). To explain all the gas observed in Coma, Trentham concluded that an $\alpha \sim -1.8$ faint end slope to the LF is required in the distant clusters, moreover this steep population should be predominantly star forming dwarf galaxies. It is therefore of considerable interest to determine observationally the form of the faint end of the galaxy luminosity function in distant clusters.

Driver et al. (1994)[DPDMD] made the first attempt to measure the faint end of the LF in a distant cluster ($z > 0.1$). Their study showed evidence for a steep slope to the LF in the range $M^* + 2$ to $M^* + 6$. Driver et al. (1994) obtained a total integration time of 2.4 ksec in *B* and *R* of a 6×4 arcmin region in the distant cluster A963 ($z = 0.206$) using the Hitchhiker parallel camera on the 4.2-m WHT. They used the data to investigate the number counts in this region and, by correcting statistically for the field contamination from counts obtained with the same instrument in a number of blank fields, they attempted to measure the cluster galaxy LF down to $R \sim 24$ (equivalent to $M^* + 6$). They found a steeply rising faint end slope, with $\alpha \sim -1.8$ in a double Schechter parametrisation. The slope of the faint end of the LF, ($d \log N/dm$) ~ 0.3 , was similar to the observed slope of the field counts. Thus their result could be reproduced by a simple zero-point shift between the magnitude scales of their field and cluster images, albeit of rather large amplitude, $\delta m \sim 0.2$. Unfortunately, owing to its operational mode the Hitchhiker system was only calibrated once a year, instrumental consistency has to be assumed, and thus it is difficult to gauge the likelihood of such an error (They quote an rms scatter on the zero point of ± 0.1 mag). To address this issue DPDMD compared their photometry with data from a shallow photographic survey which appeared to rule out any large offset.

To provide an independent check of the result reported by DPDMD we have analysed deep two colour photometry of two distant $z = 0.18$ clusters, using a similar technique to measure the cluster galaxy luminosity function. Our cluster dataset is similar in quality and depth to DPDMD's, although roughly a factor of six larger in area for each cluster than that of DPDMD. To provide field counts with the same selection criteria and conditions as our cluster images, rather than relying on published counts from the literature, we have analysed a wide-field *V* and *I* imaging survey of blank fields. In addition we have taken great care to ensure

* We adopt $q_0 = 0.5$ and $H_0 = 50 \text{ km sec}^{-1} \text{ Mpc}^{-1}$. With these parameters 1 arcsec is equivalent to 3.91 kpc at $z = 0.18$.

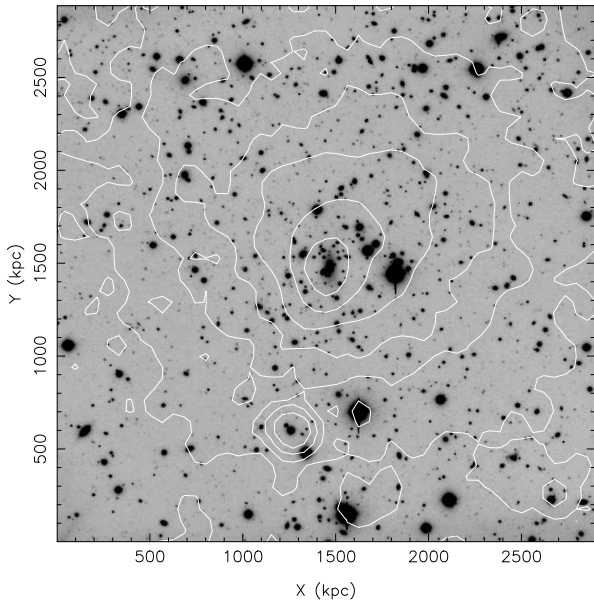


Figure 1. An I image of the rich cluster A665. The field of view is 12.3×12.3 arcmin (2.9×2.9 Mpc). North is top and East is left. Overlaid is a contour map of the X-ray emission from the cluster. The X-ray emission peaks on the central cluster galaxy and shows an asymmetric distribution with a plume off to the north-west. This structure is also visible in the distribution of red cluster galaxies.

the homogeneity of the photometric systems used for both the cluster and comparison blank fields.

We discuss our observational dataset in Section 2, present our analysis in Section 3, discuss our results in Section 4 and give our main conclusions in Section 5.

2 OBSERVATIONS AND REDUCTIONS

Before discussing our observations of the clusters and the field we first describe the general characteristics of the two clusters observed.

2.1 Cluster Properties

The two clusters analysed in this study were A665 and A1689. These clusters both lie at $z \sim 0.18$ (A665 at $z = 0.182$ and A1689 at $z = 0.181$). They are both optically rich with Abell richnesses of 5 and 4 respectively. Using our imaging data we estimate the blue fractions (f_B from Butcher & Oemler 1984) of both the clusters to be low, $f_B = -0.11 \pm 0.19$ for A665 and $f_B = 0.12 \pm 0.05$ for A1689 (c.f. $f_B = 0.09 \pm 0.03$ for A1689 from Butcher & Oemler 1984). They have somewhat different morphologies, with A665 having a single cD galaxy and A1689 containing a very dense central group of galaxies (See Figs 1 and 2). In the figures we have overlaid the ROSAT PSPC X-ray

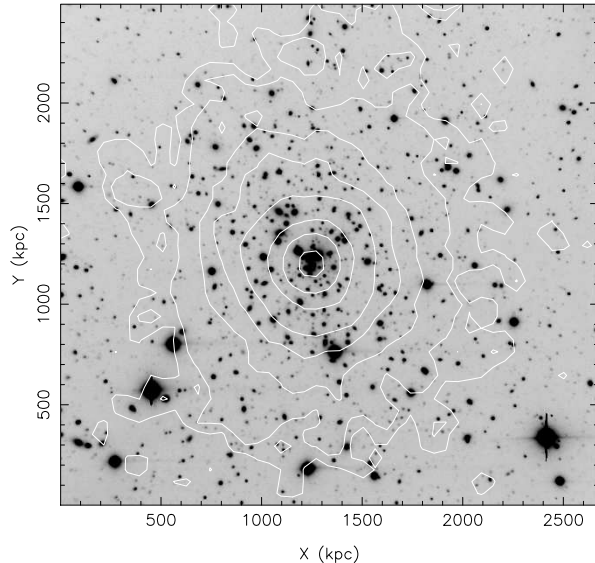


Figure 2. The I image of the cluster A1689. The field of view is 11.3×10.6 arcmin (2.6×2.5 Mpc) and North is top with East to the left. Again we have overlaid the cluster X-ray distribution as a contour map. The highly symmetrical X-ray peak coincides with the dense clump of bright galaxies which defines the cluster centre.

images taken from the ROSAT archive to illustrate the general morphologies of the clusters. The two clusters are both strong X-ray sources in the 2–10 keV band with luminosities in the 2–10 keV band of $L_X = 1.2 \times 10^{45}$ ergs sec $^{-1}$ for A665 and $L_X = 2.0 \times 10^{45}$ ergs sec $^{-1}$ for A1689 (Soltan & Henry 1983). In addition, both clusters have high velocity dispersions: $\sigma_{cl} = 1201^{+183}_{-126}$ km sec $^{-1}$ (33 members) for A665 (Oegerle et al. 1991) and $\sigma_{cl} = 1848 \pm 166$ km sec $^{-1}$ (68 members) for A1689 (Gudehus 1989). Finally, both clusters show evidence of strongly lensed features in their core regions (Tyson, Valdes, & Wenk 1990; Kaiser et al. 1994; Tyson & Fischer 1995).

The characteristics of these clusters are very similar to the cD-dominated cluster A963 studied by Driver et al. (1994). A963 is a richness class 3 cluster at $z = 0.206$ which is a strong X-ray source ($L_X = 0.95 \times 10^{45}$ ergs sec $^{-1}$, Soltan & Henry 1983) and also contains two giant arcs (Lavery & Henry 1988; Ellis et al. 1991). The cluster's blue fraction has been estimated as $f_B = 0.19 \pm 0.05$ by Butcher & Oemler (1984).

2.2 Data Acquisition

The V and I imaging of the two clusters used in our analysis was collected with the Prime Focus imager on the 2.5-m Isaac Newton Telescope (INT), La Palma. The comparison V and I observations of blank fields needed to correct for field contamination come from deep imaging with the f/1 camera on the 3.9-m Anglo-Australian Telescope (AAT), Siding Springs (See Lidman & Peterson 1996 for more de-

tails). In addition we obtained additional photometric imaging to tie the photometric systems of these two data sets together securely. These data were collected with the Prime Focus imager on the 4.2-m William Herschel Telescope (WHT), La Palma.

The imaging data on the two clusters, A665 and A1689, was collected using a $2k^2$ thick Ford CCD on the nights of 22–28 February 1993. Due to a technical problem with the data acquisition system running the Ford chip a thick $1k^2$ EEV CCD was used on the night of the 23–24 February 1993. The seeing during this run varied between 1.4–2.3 arcsec, far in excess of the limit required for the intended programme of lensing observations. Accordingly, the current project was executed as a backup programme. This involved imaging in V and I of two clusters at $z \sim 0.18$ to study their LFs over a wide-field.

Our observing technique was to take multiple exposures (each of ~ 1000 s) of the clusters, dithering the telescope by ~ 15 arcseconds between exposures. This reduced flatfielding errors and allowed us to create a master flatfield as explained in the next section. Observations of standard stars from Landolt (1992) were interspersed with the science observations throughout each night. The standards were observed across a large range in airmass to provide atmospheric extinctions and zero points for the various clusters and passbands. Furthermore, the colour range chosen for the standard stars spans the same range as expected for the cluster galaxies allowing us to determine colour-terms for the various detector and filter combinations. Two nights during the run were photometric and calibration of all passbands was made using these nights. We also corrected our magnitudes for galactic absorption (reddening) using $A_I = 0.50A_B$ and $A_V = 0.75A_B$ with A_B given by Burstein & Heiles (1984) (see Table 1).

2.3 Data Reduction

The reduction of our data followed standard procedures for the analysis of deep imaging. In particular, we chose to create super-flats using the data frames themselves to allow us to best match the characteristics of the flatfields to the science images. The reduction was all performed with standard IRAF routines and the procedure in detail was:

- (i) The frames were bias subtracted and trimmed. The median bias level was obtained from the overscan region of the chip and subtracted off. The images were then trimmed to remove the overscan strips.
- (ii) Initial flatfielding was performed using twilight flats.
- (iii) FOCAS (Valdes et al. 1983) was used to detect bright objects in the frames. These were then removed and replaced by sky values drawn from regions around the objects.
- (iv) For a given frame, all the other cleaned frames in that passband taken on the same night were median combined to create a super-flat.
- (v) The initially flatfielded frames were then flatfielded using the super-flat.
- (vi) The images were aligned and geometrically re-mapped using sub-pixel sampling to a single basis frame (centred on the cluster), and then combined using a clipped

average algorithm in the IRAF task IMCOMBINE to give final images for each passband/night.

- (vii) All final exposures from the different nights, in a given passband, were co-added to provide a single frame of each cluster in each passband.

The characteristics of the final datasets are summarised in Table 1. Our cluster data covers a region of approximately 12×12 arcmin or 2.8×2.8 Mpc in each cluster to a depth of $I \sim 22.5$ and $V \sim 24.0$. These are both equivalent to $M^* + 5$ at the cluster redshift. The average seeing ranged from 1.7 to 2.1 arcsec FWHM (Table 1). We use the mean colour of the elliptical galaxy population ($(V - I) \sim 1.5$) to determine the colour correction to transform our magnitudes onto the Landolt system. We include a contribution to the final magnitude errors from differences between the adopted colour correction and the true value arising from the observed range of galaxy colours in our fields. The final zero point errors were $\Delta I = 0.05$ and $\Delta V = 0.05$, obtained from a combination of extinction, colour and frame-to-frame errors.

2.4 Cluster Galaxy Catalogues

Having acquired and reduced our images we next needed to analyse them to provide catalogues of object positions, magnitudes and colours. To achieve this we used the SExtractor analysis package (Bertin & Arnouts 1996). This package detects objects using an isophotal threshold above the local sky (after convolution with a filter function), cataloguing those with areas exceeding a minimum value. SExtractor then deblends the objects and produces a catalogue of their properties. The object catalogue created includes information on the object positions, shapes, profiles and magnitudes. Tests to find the best detection parameters for SExtractor were run on small sections of both the V and I images of the final cluster frames. The final values we adopted are shown in Table 2. While we used SExtractor to detect objects and determine their centroids, to compare the number counts in our various fields we have chosen to use large-diameter aperture photometry (6 arcsec diameter or 23.5 kpc at the cluster distance). This photometry was performed with IRAF’s PHOT package and we discuss it in more detail later.

We corrected the catalogues for incompleteness at the faint end by means of simulations (c.f. Smail et al. 1995). We artificially generated a “typical” galaxy for each of our four cluster fields by co-adding a large number of bright galaxies ($I \sim 20$). We then scaled the flux in this “typical” object to obtain simulated galaxies of different magnitudes. We added 200 such galaxies of a fixed magnitude at a time to each of our science frames. We then re-ran SExtractor on the resulting frames and noted what percentage of the additional simulated galaxies were being missed. The simulations thus include the effects of incompleteness due to both the faintness of the galaxies and also merging with brighter objects. Note that implicit in these simulations is the assumption that, over our range of interest of 1 – 3 magnitudes, faint galaxies have similar scalelengths to their brighter counterparts. Even if this were not the case, and fainter galaxies were intrinsically smaller, the high values of seeing (~ 2

arcsec) encountered during these observations make it likely that all objects of differing magnitudes would be smoothed to a similar size. Table 1 gives the 50 per cent completeness limits of the catalogues obtained from these simulations.

To correct the catalogues for stellar contamination we have used the relation between image size and brightness to separate the stars and galaxies (c.f. Lidman & Peterson 1996). In a plot of isophotal radius versus magnitude two distinct populations are evident at bright magnitudes, with the more compact objects at any magnitude being the stars. For each frame a line separating the populations was determined visually and the objects more compact than this limit were classified as stars and removed from the counts. At faint magnitudes ($I \geq 18$) the two populations begin to merge and it is more difficult to identify the stars. Hence it seems likely that some contamination will remain, although the fraction of stellar interlopers is small. We are primarily interested in the faint end of the LF and owing to the relatively shallow star number counts compared to galaxies the star contamination becomes significantly reduced as the magnitude increases (see fig. 4 of Lidman & Peterson 1996). After star removal, the A665 and A1689 I catalogues and A665 and A1689 V catalogues contained 1689, 2035, 1659 and 1615 objects above their respective 50 per cent completeness limits.

Before discussing the field counts used to correct our cluster observations we first discuss whether the SExtractor detection parameters that we used might cause us to miss a population of low surface brightness galaxies.

2.5 Are Low Surface Brightness Galaxies Being Missed?

CCD frames are less susceptible to missing low surface brightness objects than photographic plates (see e.g. Bernstein et al. 1996 and Turner et al. 1993 for more discussion). Despite this, and to test the sensitivity of our object detection algorithm to the adopted surface brightness limit, we also catalogued our cluster frames using a procedure similar to that used by DPDMD in their analysis of A963. We selected a very low surface brightness limit for our object detection with the understanding that the ensuing sample would be strongly contaminated by noise objects. Rather than making an arbitrary choice for the detection threshold we chose to vary its value in the range 1.0-2.0 σ and selected the level which produced the highest number of new detections. This is not simply the lowest threshold, owing to the effects of the deblending algorithm on merged galaxy images.

To determine the excess number of real objects not detected by our standard procedure we first removed all those objects from the low-threshold (LSB) I catalogues which occurred in the standard versions of the catalogues. Next we used the fact that the reddest galaxies expected at the cluster redshifts ($z = 0.18$) will correspond to the colours of the spheroidal populations (E/S0) of the cluster ($(V - I) \sim 1.6$). Thus any real cluster objects will have colours bluer than $(V - I) \leq 1.6$ measured from the seeing-matched V and I images, or for our limiting magnitudes of $I = 22.0$ and $I = 22.5$ they would have $V \leq 23.5$ and 24.0 respectively.

The number of objects from the LSB catalogues which are brighter than $I = 22.0$ (22.5), are undetected using the standard algorithm, and yet have V magnitudes brighter than $V = 23.5$ (24.0) was 50 in A665 (2.5 per cent of the whole population) and 33 in A1689 (1.4 per cent) respectively. These proportions make a negligible difference to the cluster LF discussed later and so we conclude that our standard object algorithm is not significantly biasing the object catalogue against low surface brightness cluster members, in so far as they are detectable in our data.

2.6 AAT f/1 Field Imaging

The blank field observations necessary to field-correct our cluster counts come from a wide-field V and I CCD survey of the equatorial LDSS fields at 10^{hrs} and 13^{hrs}. The detector was a 1k² Thomson CCD with 0.98 arcsec/pixel sampling, providing a large field of view ($\sim 17 \times 17$ arcmin). The data were all taken in photometric conditions and in seeing comparable to that encountered for our cluster observations. These data were kindly supplied and reduced by Dr. C. Lidman. Dr. Lidman also provided internal calibrations between the various fields with estimated internal zero point errors of $\Delta \sim 0.03$ (Lidman & Peterson 1996).

2.7 Calibration of the Comparison Field Photometry

This final imaging dataset was acquired to tie the AAT and INT frames rigorously to a single photometric system. While both catalogs claim to be on the Landolt (1992), it appeared prudent to us to actually test this claim. For this purpose the INT cluster fields and a selection of the AAT blank fields were re-observed with a 1k² thinned Tek-2 chip on the Prime Focus Imaging Facility of the WHT. The conditions were photometric but the seeing was very poor ($\simeq 4$ arcsec). Observations of Landolt (1992) standard stars across a wide range in airmasses were also taken to provide robust photometric transformations. The science frames were reduced in a standard manner using twilight flatfields before being rebinned to either the INT (for cluster) or AAT (for field) pixel scales. The INT and AAT data were degraded to the same seeing as the WHT and 10 arcsec diameter aperture magnitudes then measured from galaxies in the fields. We determine magnitude offsets for the AAT data relative to the INT cluster fields. The AAT field data was deemed to have magnitude offsets of $\Delta(I_{AAT} - I) = 0.07 \pm 0.05$ and $\Delta(V_{AAT} - V) = 0.14 \pm 0.07$ relative to the INT system. The relatively large offset uncovered in the V band is disappointing given the claimed accuracy of the two catalogs, but we reiterate that it was to check for exactly this sort of problem that we undertook these observations. The source of this offset has proved difficult to track down. One check on the relative magnitude scales in the INT cluster data is available from the colours of the E/S0 sequence, this has a mean colour of $(V - I) = 1.51$ at $V = 17.2$ with a scatter of $\delta(V - I) = 0.05$ in both clusters. This is in reasonable agreement with the no evolution predicted colour of $(V - I) = 1.57$, indicating that the INT photometric is likely to have offsets of ≤ 0.06 .

We applied corrections to the field catalogues to put the field and cluster photometry all onto the INT system. By performing this calibration of our control fields we were able to ensure that the relative zero point errors between our cluster and field photometry were reduced to a minimum (~ 5 per cent random errors).

2.8 Field Catalogues

We analysed the AAT imaging data as in Section 2.4, with equivalent selection criteria. In our analysis we chose to use 9 I fields (with seeing less than 2.1 arcsec) and 4 V fields (with seeing less than 2.6 arcsec). We employed similar simulations to those described in Section 2.4 to correct for incompleteness, this time generating a typical galaxy for each passband (the observing conditions and, in particular, the seeing for all the data frames taken with each filter was approximately similar so it was only deemed necessary to perform incompleteness simulations using one representative frame in each passband). The AAT field survey provided adequate statistics for number counts as faint as $I \sim 22$ and $V \sim 22$, close to the limiting magnitudes of our cluster datasets. Again, we isolated and then removed the stars by plotting isophotal radius versus magnitude.

To measure the magnitudes of the objects on the cluster and comparison fields we chose to use simple aperture magnitudes. To provide reasonable estimates of “total” magnitudes these were measured in 6 arcsec diameter apertures centred on the object positions provided in the SExtractor catalogues. The background sky was measured in a wide surrounding annulus. To remove differential aperture corrections between the datasets we convolved all the images in a particular passband to the seeing of the worst, using a Gaussian filter, before measuring aperture photometry with IRAF’s PHOT package.

In our analysis we have chosen to fit a single power law to the observed field counts. We used a maximum-likelihood technique, based on minimising χ^2 to determine the slope (γ) and intercept (C_m) of the power law fit. The differential counts per square degree per 0.5 magnitude were found to be:

$$\log_{10} dN = (0.331 \pm 0.018)I - (3.24 \pm 0.40) \quad (2.1)$$

$$\log_{10} dN = (0.377 \pm 0.028)V - (4.73 \pm 0.63) \quad (2.2)$$

over the range 19.0–22.0 for I and 19.5–22.0 for V (the mean, and upper and lower limits on the counts are shown by the solid lines in Fig. 3). The errors in the slope and normalisation are composed of two components, errors in the fit and frame-to-frame errors caused by Poissonian fluctuations between frames. Our slopes are in reasonable agreement with those published previously by DPDM $\gamma_I = 0.34 \pm 0.03$ ($I = 19.0$ – 22.5) and $\gamma_V = 0.41 \pm 0.01$ ($V = 20.5$ – 23.0). Furthermore, the number counts have been found to rise linearly in these passbands to much fainter magnitudes (see e.g. Smail et al. 1995) and so we feel confident in marginally extrapolating our field counts to obtain the same depth as used in the cluster analysis.

At this point we wish to quantify the effect gravitational lensing by the clusters will have on the surface density of

background galaxies seen through the cluster. Both clusters are known to be strong gravitational lenses and they have the potential to increase or decrease the observed surface densities of galaxies seen through them (Broadhurst 1996). Two competing effects are present: the light paths to distant galaxies are deflected by the cluster, resulting in their images being displaced radially outward from the cluster centre (effectively lowering the background surface density), meanwhile faint galaxies are brightened by the lensing amplification above our magnitude limit. Using the methodology of Broadhurst (1996), we expect the observed number density of galaxies, N' , to be related to the number density of galaxies in the absence of the cluster, N_0 , by:

$$\frac{N'}{N_0} = A^{2.5s-1} \quad (2.3)$$

where A is the amplification and s is the slope of the field counts. Using a singular isothermal sphere approximation to the cluster potential and our V and I band field count slopes of 0.377 and 0.331, we would expect to find a deficit of 2.5 per cent and 7 per cent respectively in the background population in each passband for our fieldsize. These effects are negligible compared with the field-to-field scatter and so we will ignore lensing in the ensuing discussion.

3 ANALYSIS

In summary, we have measured the differential galaxy counts in our cluster fields and we have discussed the photometric zero point offsets applied to the AAT catalogues to ensure consistency of photometry between the AAT and INT datasets. We have determined power law fits to the background field counts and hence we are now in a position to subtract the number of background galaxies statistically as a function of magnitude from the total number of galaxies in our cluster fields, to leave only the cluster members. In the following sections we will firstly fit single Schechter functions to our cluster luminosity functions as is customary, before going on to show that improved fits may be obtained using combined Gaussian+Schechter functions.

3.1 Measuring the Luminosity Functions

We show the field-corrected cluster LFs for the clusters in both passbands in Fig. 4. These include corrections for incompleteness in the cluster frames. One additional systematic effect remained which had to be corrected for: in a crowded cluster field there is less open area available in which to detect the fainter galaxies than in the corresponding field sample and so some faint background objects will be obscured by brighter galaxies (as opposed to just having merged isophotes). This effect will also occur in the field but will be less important. We attempted to correct for this by computing the available clear field of view for each magnitude interval by subtracting from the total frame area the area covered by brighter galaxies. This technique will slightly overestimate the compensation factor required, because it assumes that *all* faint objects which happen to occupy the

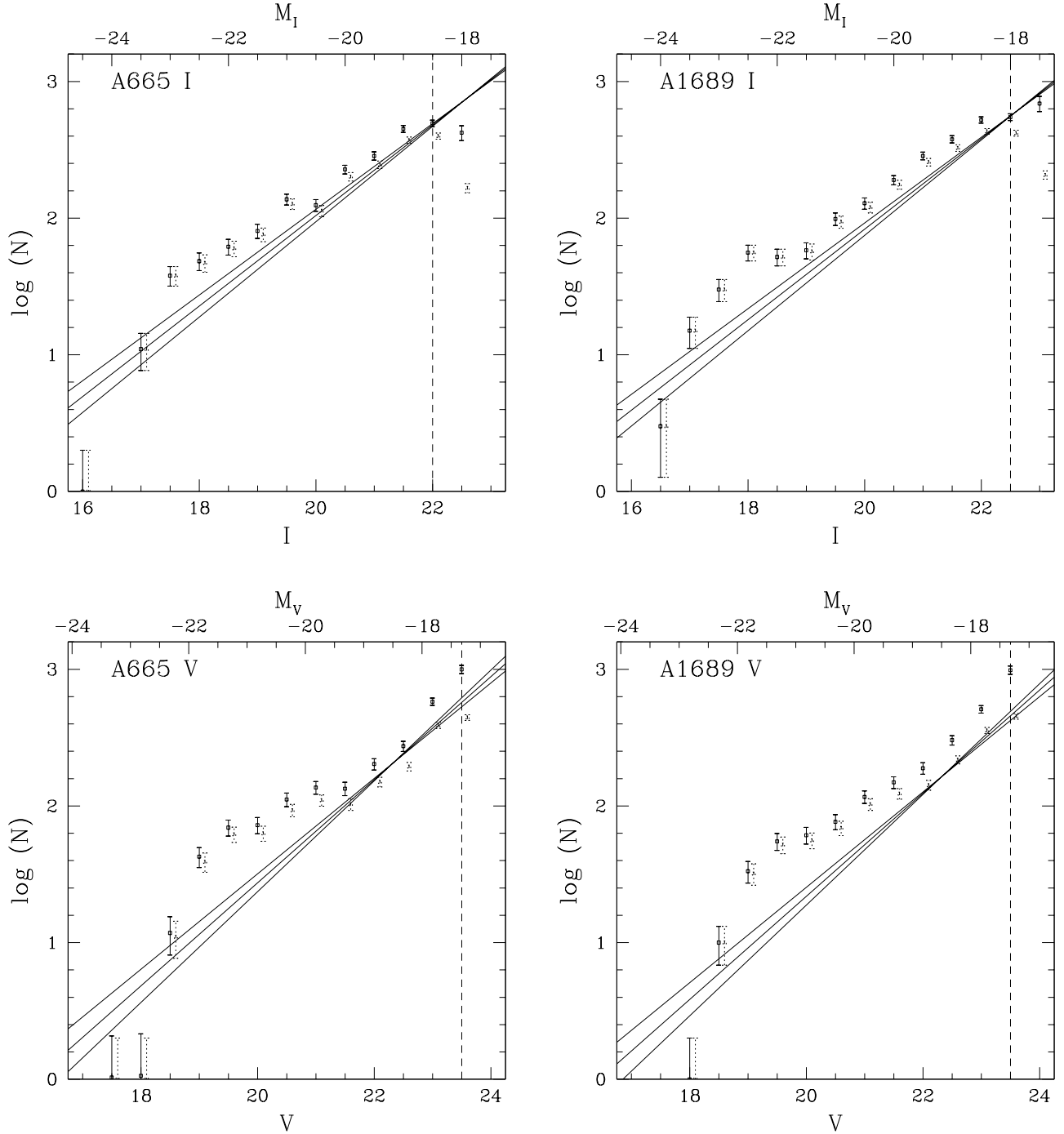


Figure 3. Number counts for the I (upper) and V (lower) images of the two clusters. The counts are per field of view area for each cluster (Table 1) and per 0.5 magnitude bin. The solid points have been corrected for incompleteness, the dotted points are the uncorrected counts offset by 0.1 mag for clarity. The equivalent field counts from the AAT f/1 data are overlaid. The three solid lines show the best fit to the field counts and the $\pm 1\sigma$ errors. The dashed line shows the 50 per cent incompleteness limit. Note the excess in the cluster at $I \sim 17$ and $V \sim 18.5$ associated with the onset of the bright cluster population. Stars have been removed from all the counts.

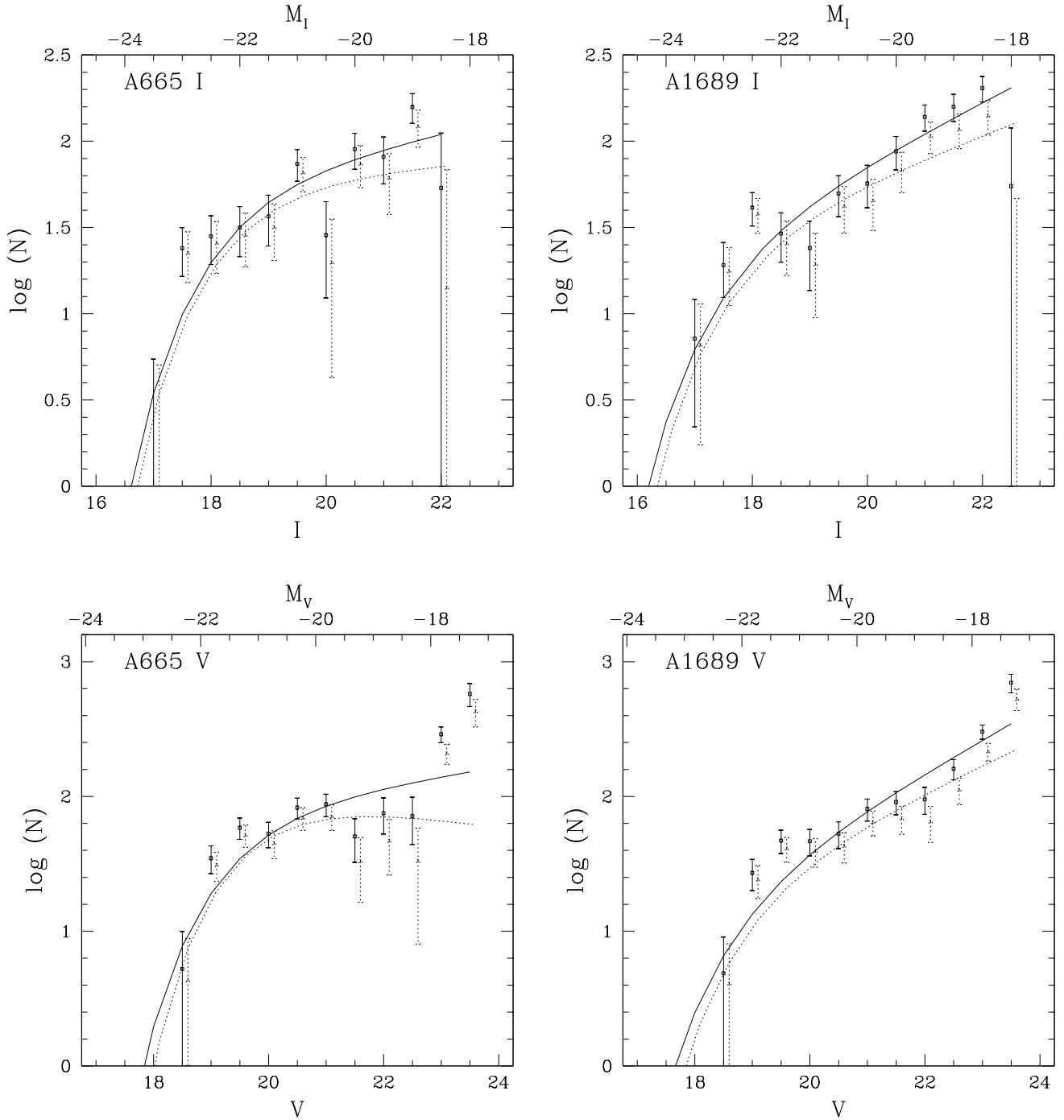


Figure 4. Field corrected cluster LFs, defined as number of galaxies per field per 0.5 mag. The solid points and line have been corrected for both incompleteness and obscuration by brighter objects (see text), while the dotted points and line are only corrected for incompleteness and have been offset by 0.1 mag for clarity. Overlaid are the best fit Schechter functions for each cluster. The parameters are given in Tables 3 and 4.

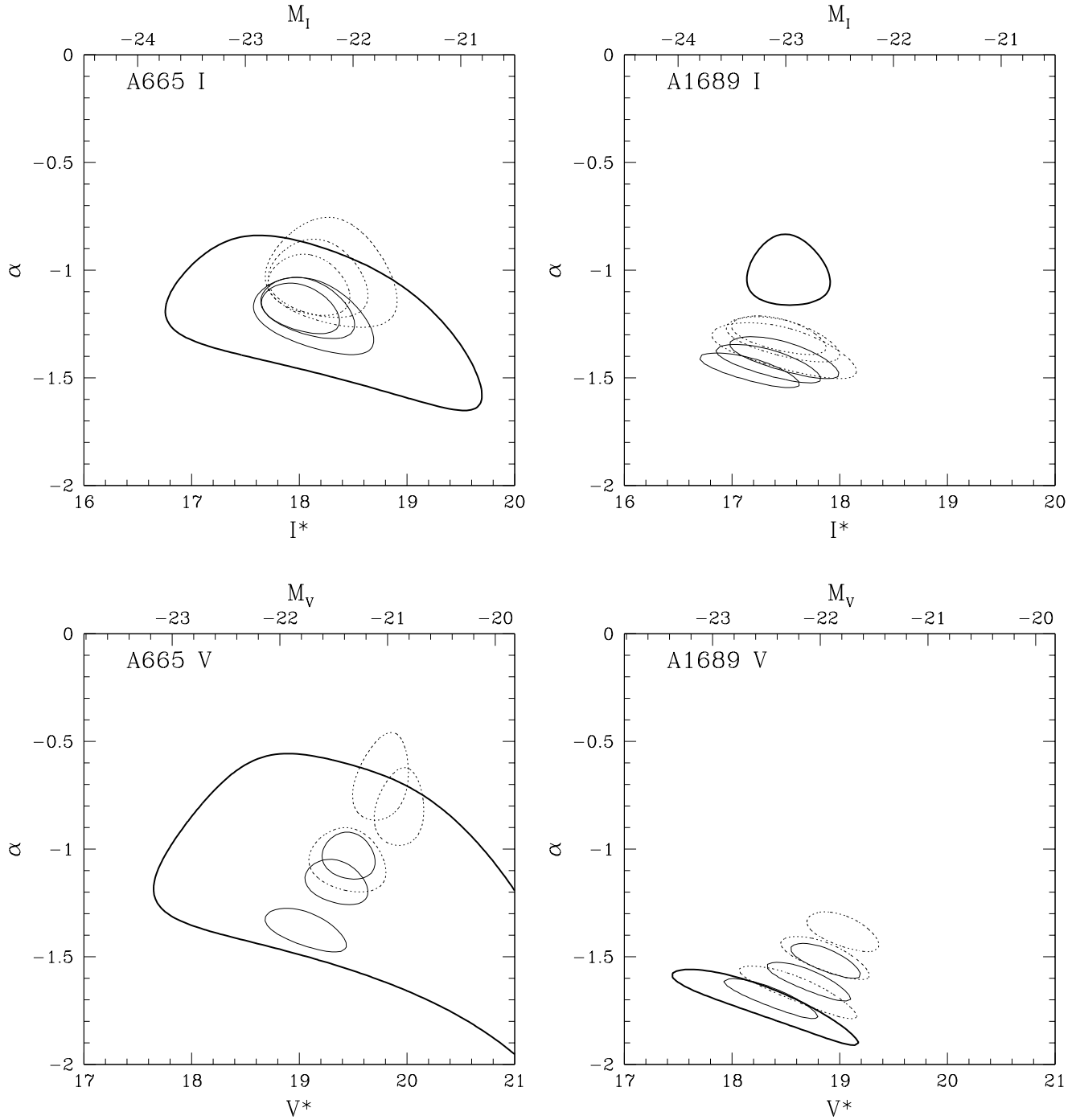


Figure 5. α and M^* error contours. The contours are $\chi_{\min}^2 + 6.3$ which corresponds to a 90 per cent confidence ellipse for normally-distributed errors and three free parameters. The solid lines are from a Schechter fit to the incompleteness and obscuration corrected points. There are three lines corresponding to the best and extreme ($\pm 1\sigma$) values of the power law fits to the field counts. The dotted lines are from a Schechter fit to the incompleteness only corrected points. The bold line is from a Schechter fit to the incompleteness and obscuration corrected inner/outer test points.

same region of sky as a brighter counterpart will be obscured i.e. that the bright galaxies are “optically-thick” at their isophotal diameter. The “true” obscuration correction will depend on the surface brightness distributions in the bright and faint galaxies, the internal extinction distribution in the bright galaxies and the properties of the detection algorithm. We claim, therefore, that the two limits we use (no correction and the optically-thick case) span the likely range.

As for the field counts, we again used a maximum-likelihood method based on chi-squared to measure the α , M^* and N^* parameters in the Schechter function,

$$N(M) dM = kN^* e^{k(\alpha+1)(M^*-M)} e^{-e^{k(M^*-M)}} dM \quad (3.1)$$

where $k = \frac{2}{5} \times (\ln 10)$.

The generalised chi-squared statistic used was

$$\chi^2 = \sum_i \left(\frac{\log_{10} N_O(i) - \log_{10} N_E(i)}{\sigma(i)} \right)^2, \quad (3.2)$$

where $N_E(i)$ is the number of galaxies expected from the Schechter function in the i ’th bin, and $N_O(i)$ is the number observed. $\sigma(i)$ is the error for each bin, namely, the Poisson error in the cluster-plus-field counts and the Poisson error in the field counts, added in quadrature. In addition, we have chosen to double the error for the final bin to reflect the greater uncertainties associated with final point measurements and correction values.

As a simple estimate of the scatter in the Schechter fit due to uncertainties in the field counts, we fit for our Schechter parameters three times, subtracting firstly the field counts derived from our best fit field slope and normalisation parameters, and then the extreme ($\pm 1\sigma$ values) (from equations 2.1 and 2.2). This gives three best fit values for the three cases. As the Schechter function involves three parameters, the confidence contours are three-dimensional shapes. The dotted lines in Fig. 5 show one slice through each 3-D contour shape (N^* is held constant at its most likely value). Ellipses corresponding to $\chi^2_{\min} + 6.3$ (the 90 per cent confidence level for normally distributed errors with three degrees of freedom) error contour are marked. The most likely values of the Schechter parameters are shown in Table 3. The function itself is shown in Fig. 4 (solid for both incompleteness and obscuration corrected versions and dotted for incompleteness corrected only). To convert from apparent to absolute magnitudes we used $M = m - 5 \log_{10} D - 25 - K$ where D is the luminosity distance to the cluster ($H_0 = 50 \text{ kms}^{-1} \text{ Mpc}^{-1}$) and K is the K-correction for E/S0 galaxies (calculated by convolving our filter responses with the spectral energy distribution of a present-day elliptical galaxy redshifted to $z = 0.18$). The combined K-correction and distance modulus, $m - M$, is 40.50 in I and 40.82 in V .

3.2 Independent Comparison Check

We next determined a rough estimate of the cluster LF which was entirely independent of the relative magnitude scales of the cluster and field data. Here we took advantage of the large field of view available in our clusters and the strongly peaked distribution expected for galaxies bound to

the cluster potential. We split our cluster frames into two independent radial bins, each covering the same chip area. For the various images this translated into radii of ~ 0 –0.9 Mpc and ~ 0.9 –1.3 Mpc. We then simply subtracted the differential counts in the outer region from those in the inner one. This would completely remove any galaxy population which has a flat distribution across the frame, i.e. the field population, and leave only the peaked cluster galaxies. In the absence of luminosity segregation within the clusters, the resulting magnitude distribution of galaxies would represent the global LF of the cluster.[†]

We show the results of this analysis in Fig. 6. The solid points and line have been corrected for both incompleteness and obscuration by brighter objects, while the dotted points and line have only been corrected for incompleteness and are offset by 0.1 mag for clarity. Overlaid on Fig. 6 is the best fit Schechter function. The parameters are given in Table 5. Note that we might expect to obtain a smaller value for N^* , the normalisation, using this method, compared to the value obtained in the field subtraction case. This is because some fraction of cluster galaxies will be located in the outer annulus and will be subtracted from the total along with the field galaxies. We see by comparing values of N^* from Tables 4 and 5 that this is indeed the case.

The bold lines in Fig. 5 show one slice through each error fit to a Schechter function for the incompleteness and area corrected points. The errors are much larger for this test than the field-subtraction one, but we reiterate that as a differential test this is not affected by a zero-point magnitude error and is sensitive to any population of clustered galaxies centred on the cluster centre.

4 RESULTS AND DISCUSSION

In Fig. 4 we showed the best fit Schechter functions including both incompleteness and area corrections. In Fig. 6 we showed the results of an independent, if less sensitive test. In Fig. 5 we made a quantitative comparison of the various fits by displaying the error contours associated with each of the distributions. Comparing the A665 and A1689 V and I error distributions in Fig. 5 with each other it is clear that the best fit parameters for a single Schechter function are only in very rough agreement, both between the clusters and for the various fits within each cluster. This is surprising given the apparent similarity of the LFs in Fig. 4. The reason for this is apparent when we compare the best fit Schechter functions to the data, especially the V data. Both clusters exhibit a faint component which rises very rapidly at faint limits (The coarser binning and lower signal to noise in the inner/outer comparison smears out this component and results in a generally steeper faint end slope to the fits). A single Schechter function is incapable of simultaneously fitting both this feature and the bright end of the LF, as is shown

[†] We have tested for luminosity segregation (Lobo et al. 1996) by combining the LFs in the inner and outer regions of the two clusters and find only weak evidence for a steepening of the faint end slope α with radius in the clusters.

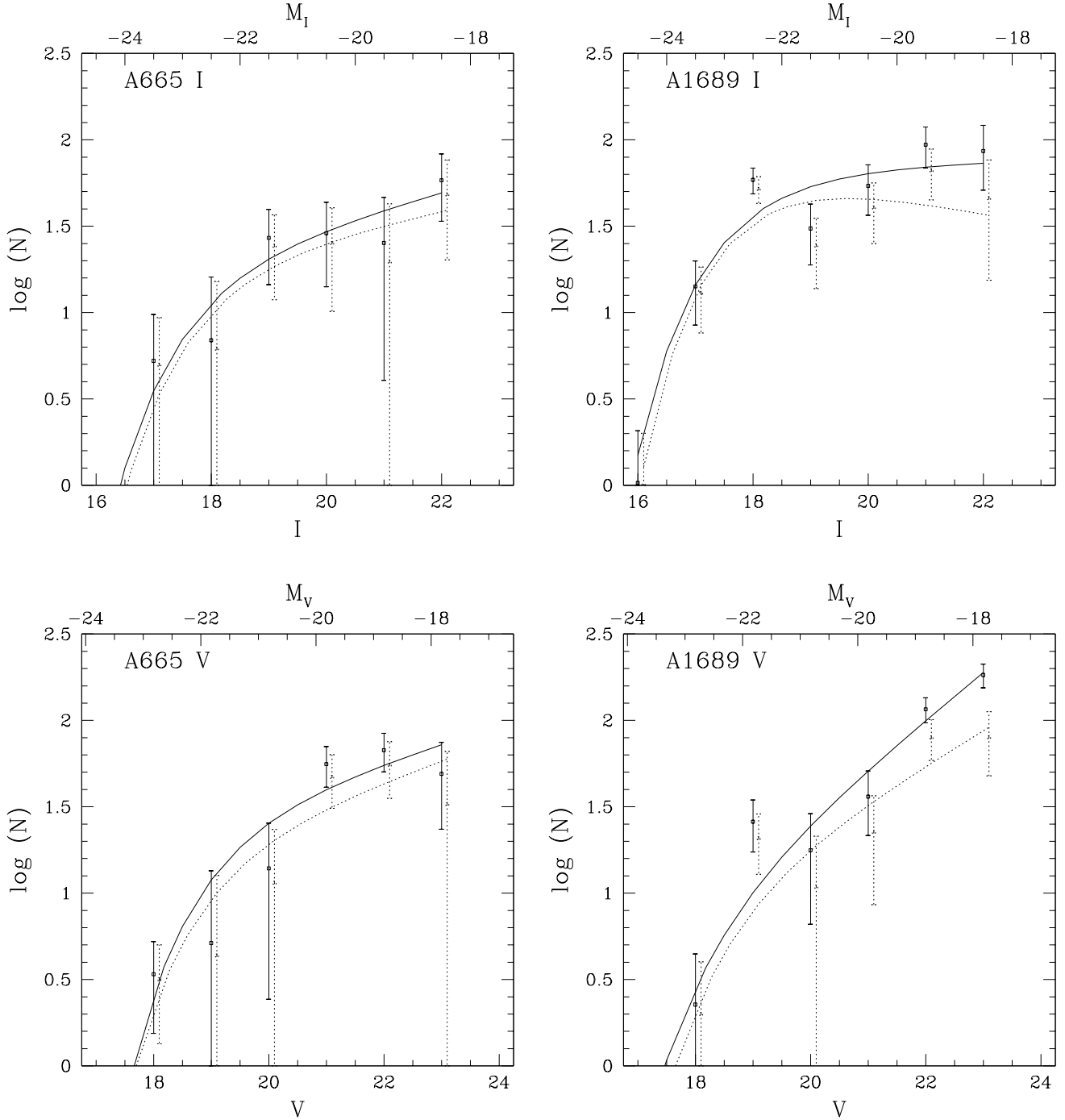


Figure 6. Estimates of the cluster LFs obtained from differential counts between the central and outer regions of each cluster. The solid points and line have been corrected for both incompleteness and obscuration by brighter objects (see text). The dotted points and line have been corrected for incompleteness only and offset by 0.1 mag for clarity. Overlaid are the best fit Schechter functions for each case. The parameters for the incompleteness and obscuration corrected fits are given in Table 5.

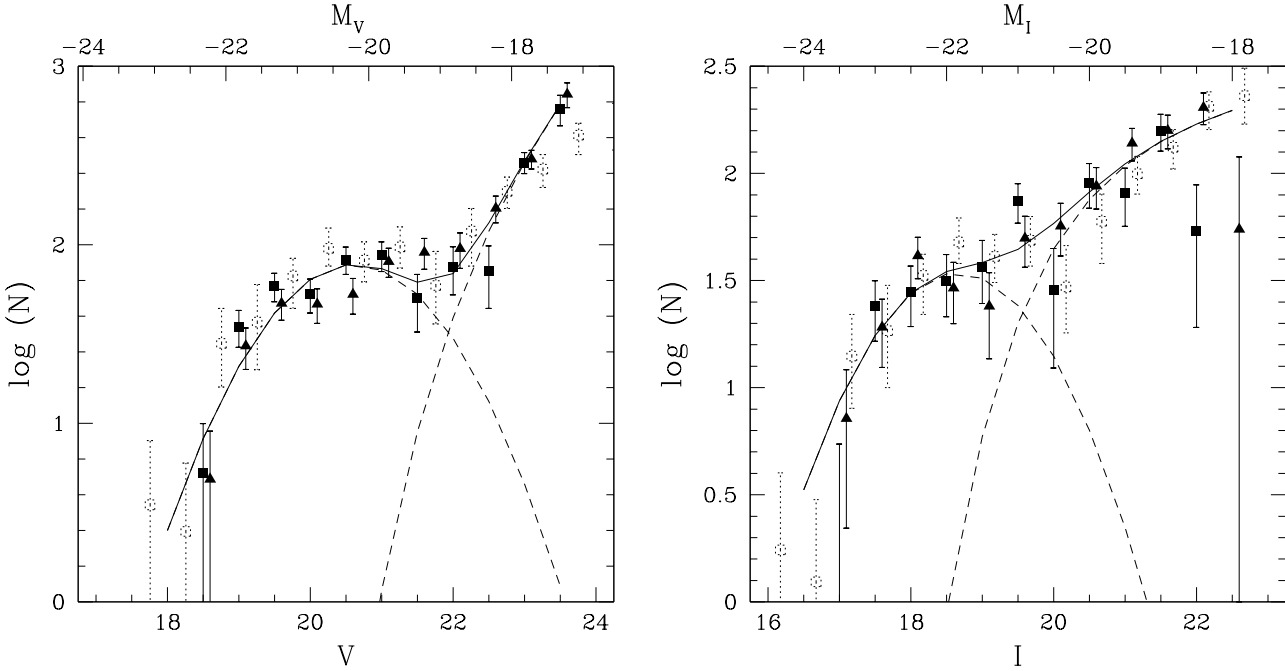


Figure 7. Incompleteness and obscuration corrected points for A665 (solid squares) and A1689 (solid triangles). Also shown (open squares) is the data from Driver et al (1994) which has been scaled as described in the text. Overlaid to our data is the best fit Gaussian+Schechter function (See Table 6 for the parameters). The A1689 data and line has been offset by 0.1 mag. Note the good agreement between the form of the LF in the three clusters.

by the reduced χ^2/ν values for the fits listed in Table 4. These range between 2.1 and 6.6 and indicate that a single Schechter function is a poor analytic fit to our data points. The disagreement between the fits for the two clusters thus arises from the combination of the incorrect functional form for the LF and the different contributions of the faint component to the fit due to the slightly different magnitude limits of the datasets.

In order to decide upon a better functional form to describe the observed LFs we again plot our V and I data in Fig. 7. The A1689 data has been displaced (solid triangles) by 0.1 mag from the A665 data (solid squares). However, it was not necessary to scale the data vertically (i.e. both clusters are of approximately equal richness). DPDMD’s A963 R data is also shown displaced and overlaid (open squares). We have applied a combined ($V - R$) colour and distance modulus displacement of +0.51 for E/S0 galaxies ($(R - I)$ of 1.08), and also an empirical normalisation constant. The very close similarity between the shapes of the three functions is immediately apparent, with all three functions exhibiting a Schechter function form at the bright end and then evidence for an upturn at magnitudes fainter than $V \sim 22$ ($I \sim 20$). In the following discussion we will focus on the V data where this upturn is more prominent.

In the paper of DPDMD it was also noted that the upturn at the faint end ensured that a single Schechter function was not a satisfactory fit to the data. DPDMD decided to fit a double Schechter function to their data, fixing the slope

of the first function (with the brighter knee) to be equal to -1.0 . Here, instead, we elected to fit a combination of a Gaussian function at the bright end of the form:

$$N(M) = K e^{-(M-M^{\text{cent}})^2/2\sigma^2} \quad (4.1)$$

and a Schechter function given by equation 3.1 at the faint end. We prefer this description over the double Schechter function as it has been used extensively in investigations of the LFs of local clusters (e.g. Metcalfe 1983; Secker & Harris 1996; Thompson & Gregory 1993; Biviano et al. 1995), including morphological studies (e.g. Binggeli et al. 1985) which have shown that giant galaxies tend to follow a Gaussian distribution and dwarfs a Schechter function.

As there is some degeneracy between the various parameters we have elected to fix the the peak of the Gaussian, K , to be 10 per cent of the normalisation, N^* , of the Schechter function (reasonable values lie in the range 0.08 – 0.14). We also chose to fix the standard deviation of the Gaussian to be $\sigma = 1.0$, in keeping with values determined locally for Coma (Metcalfe 1983; Biviano et al. 1995; Secker & Harris 1996). Table 6 gives the best fit parameters for the Gaussian+Schechter function description of the individual cluster LFs, as well as those for the samples without the obscuration correction. As is apparent, this function provides a much better description of the data than a single Schechter function. This is supported by the reduced χ^2 values for the Gaussian+Schechter fits which are all significantly better than the single Schechter fits (Table 4). The reduced

χ^2 values are still higher than might be expected, although we have not allowed for the effects of clustering and have low numbers of objects in our bright bins. Nevertheless, the Gaussian+Schechter fits allows us to make a robust quantitative comparison of the form of the LFs in the two clusters.

We see from Table 6 that there is remarkable consistency between the M^{cent} and M^* values for each bandpass. In the V band, M^{cent} is -20.27 for A665 and -20.19 for A1689, and in I it is -22.14 for A665 and -22.06 for A1689. There is also close agreement between the values of M^* , with -18.13 for A665 and -18.50 for A1689 in V , and -20.49 for A665 and -20.47 for A1689 in I . In view of this good agreement between the two clusters we therefore combined their LFs and show the fit to this combined dataset in Fig. 7. The parameters used may be found in Table 6.

The main point of interest in comparing the cluster luminosity functions in V and I is the much steeper faint end slope in V compared to I . This difference implies that fainter cluster galaxies must have colours which are significantly bluer than the bright ellipticals. In order to quantify this effect we plotted the cumulative number of galaxies (using our best Gaussian+Schechter fits) in each passband as a function of magnitude. If both passbands were detecting the same objects then comparing the magnitude limits in V and I as a function of cumulative density would give the typical colours as a function of magnitude in the population. We found that the mean $(V - I)$ shifts from $(V - I) \sim 1.6$ at $I \sim 16$ (the colour of the bright cluster ellipticals) to $(V - I) \sim 0.6$ by $I = 22$ ($M = -18.5$). The steady blueing of the cluster elliptical population as a function of magnitude, presumably due to metallicity effects, amounted to only $d(V - I)/dI = 0.07$ per mag, and so can only account for half of the colour shift. Thus the difference in the faint end slopes in the V and I passbands apparently reflects a rapid blueing trend in the faint galaxy population in the clusters, with the faintest cluster members having the colours and luminosities of typical dIrr galaxies.

As we discussed earlier, the Gaussian+Schechter parameterisation has been used to describe the LF of the Coma cluster (an Abell richness class 2 cluster). Here, we compare the properties of the bright galaxy populations in our distant clusters, as described by the Gaussian component, with those seen in Coma. The value of M^{cent} for our combined cluster sample is $M^{\text{cent}} = -20.20$ in V , very close to that found for Coma: -20.03 (Thompson & Gregory 1993), -20.20 (Biviano et al. 1995) and -20.16 (Secker & Harris 1996) (converting all measurements to the V band using $(B - V) = 1.0$). The scatter amongst the various analyses of Coma indicates that we ought not to put too much weight on this comparison, but it is interesting to note that the distant clusters appear to be ~ 0.1 brighter in rest-frame V compared to the local value. This degree of brightening is not unreasonable out to $z = 0.18$ in a population of passively evolving elliptical galaxies formed at high redshift (Barger et al. 1996).

Turning to the faint cluster population, parameterised by the Schechter function, we find that locally the values of the characteristic luminosity M^* are more poorly defined and have larger errors; -18.1 (Biviano et al.), -18.7 (Secker & Harris) and -18.0 for the dE population in the Virgo clus-

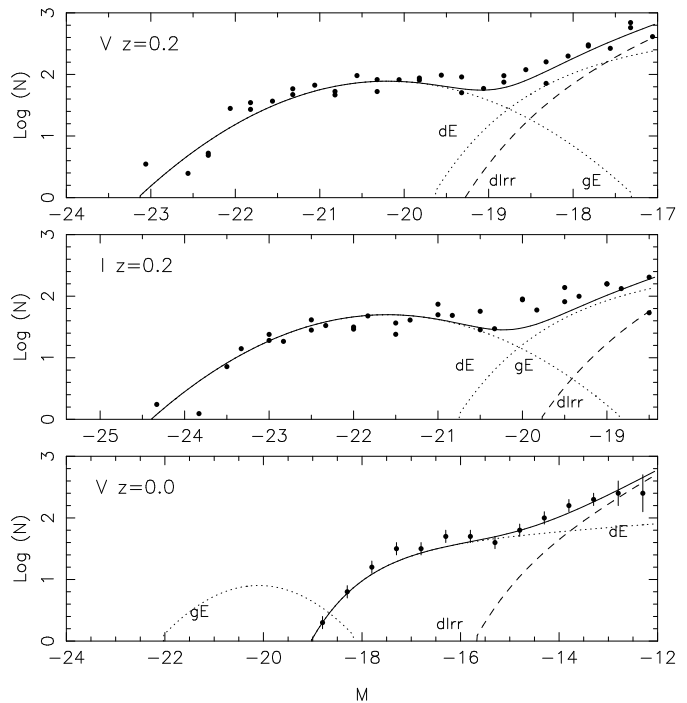


Figure 8. Our simple model for LF evolution in clusters. The composite LF of the cluster is shown by the solid line (except for the $z = 0$ case where we show the composite dwarf LF), the various sub-components are shown by dotted/dashed lines. Overlaid on these are the observed data points from Fig. 7. We show in the bottom panel the dwarf elliptical LF derived for Virgo by Impey et al. (1988) converted into V using $(B - V) = 0.6$ (applicable to dEs), where we have increased the size of the error bars at the faint end to take into account the uncertainties in the corrections applied by Impey et al.

ter (Binggeli et al. 1985). Again these encompass the value observed in our distant clusters, $M^* = -18.5$, indicating a similar lack of strong evolution in the characteristic luminosity of this population to that seen for the brighter galaxies. However, when we compare the faint end slope, α , for the faint cluster population we find a large difference between the distant and local clusters. The faint end slope in Coma lies in the range $\sim -1.1 - -1.4$ (Biviano et al. and Secker & Harris) and possibly even steeper ($\alpha \sim -1.7$ for the dE population of Virgo (Impey et al. 1988)), compared to $\alpha \sim -2$ for our distant clusters \ddagger .

The consistency of the upturn at the faint end in the three clusters available to us, particularly in the V band, suggests that this feature is common to many distant rich clusters. The fact that the upturn appears much less dramatic in the I band indicates that faint end population is significantly bluer than the typical bright cluster galaxies. To obtain an overview of the implications of these observations we have constructed a simple model which takes the

\ddagger The divergent slope found in our fits can easily be reduced by selecting a different characteristic luminosity in the Schechter part of the LF.

broad features of the observed $z \sim 0.2$ V band LF discussed above and predicts both the $z \sim 0.2$ I band LF and the evolved V band LF which we would expect to observe locally. The key feature of this model is the division of the faint component of the cluster LF into two equal populations, dwarf ellipticals (dE) and dwarf irregulars (dIrr). The LFs for both of these groups follow a Schechter form, but the different star formation histories expected for the two populations result in significantly different evolution to the present day.

In the top panel of Fig. 8 we replot our V band data from Fig. 7. We also show the constituent LFs of the three populations assumed in our simple model, and the resultant LF. The giant elliptical galaxies (gE) have been assigned the same M^{cent} and N^* values as discussed in Table 6. The dwarf elliptical and dwarf irregular populations have equal normalisations and characteristic luminosities ($M_V \sim -17.8$) but have radically different faint end slopes. The dwarf ellipticals have been assigned a value of $\alpha \sim -1.2$ (chosen because this was the value observed for our I band LF). The dwarf irregular population has a much more steeply rising slope (with $\alpha \sim -2$).

We next used the colours expected for these three populations to predict the expected form of the $z \sim 0.2$ I band LF. We used the observed colours of the giant and dwarf ellipticals taken from fits to the E/S0 sequence in the clusters and estimated at their characteristic magnitudes ($(V - I) \sim 1.5$ for Es, and $(V - I) \sim 1.2$ for dEs) to transform their LFs from V to I . For the dIrr population we adopted the colour of a dIrr galaxy (close to flat spectrum), $(V - I) \sim 0.6$. The three transformed LFs are shown in Fig. 8, as is the expected composite I band LF. As can be seen this is in reasonable agreement with the observations which we have overplotted.

Finally we used our model to predict what present day V band LF we might expect to observe in a rich cluster. The two faint end populations will evolve very differently with time. The dwarf ellipticals will evolve passively in a similar manner to the bright cluster ellipticals (with fading by about 0.1 mags in rest-frame V between $z = 0.2$ and today). The very blue (star forming) dwarf irregulars, however, are assumed to have their star formation stopped soon after we observe them (around ~ 3 Gyrs ago), either due to a violent truncation mechanism (such as ram-pressure stripping of their disks or a galactic wind) or by the slower removal of the gas-reservoirs in their halos. This population will then fade rapidly (by upwards of 2–3 mags in rest-frame V (Barger et al. 1996), and possibly up to ~ 5 mag (Babul & Ferguson 1996)). An even more drastic possibility would be that the galaxies are partially or totally disrupted due to tidal interactions in the cluster and either become low surface brightness dwarfs (the blue and hence relatively young objects discovered in Virgo by Impey et al. (1988) or be removed from the scene altogether (c.f. Babul & Rees 1992). Whatever the mechanism, the dwarf irregulars are assumed to have faded dramatically (3 mags) by the present day. We show the individual LFs in the bottom panel of Fig. 8 and also the composite dwarf LF (the faded dIrr+dE population). We have also plotted in Fig. 8 the Impey et al. LF of dwarf ellipticals in the Virgo cluster. Clearly, this can be ad-

equately described using our combined dwarf population. It is interesting to note also that the region around $M_V \sim -16$ where the dIrr begin to appear in reasonable numbers is also the point at which Impey et al. report the breakdown in the surface-brightness–luminosity correlation in their data, indicating that these fainter objects probably arise from a very mixed group of progenitors.

In summary, the significant difference in the colours of the dwarf ellipticals and dwarf irregulars implies that the former dominate in the I band LF of the distant clusters to the limit of our data (although not much fainter) and the latter determine the faint end in the V band. The differential evolution in the dwarf irregulars results in them fading far down the LF by the present day – leaving the intermediate regime $M_V \sim -18$ dominated by the dwarf ellipticals. Below $M_V \sim -16$ remnants of the dwarf irregulars begin to be seen in large numbers resulting in an upturn in the LF.

Finally, we used our model to predict the early-type dwarf to giant galaxy ratio (EDGR) in our distant clusters. Local studies i.e. Secker & Harris (1996) find an EDGR of 1.8 ± 0.6 in the Coma cluster to a limit of $M_B = -15.5$ ($M_V \sim -16.1$), similar to the value of 2.1 found for Virgo by Ferguson & Sandage (1991). Note that we compared our results only with the brightest subsample from Secker & Harris and Ferguson & Sandage because this required the least extrapolation beyond the limit of our data. If we calculate the EDGR from the dE and gE populations in our model at $z \sim 0.2$, we obtain an EDGR of 2.3 for $(K/N^*) = 0.1$ (ranging from 3.3 for $(K/N^*) = 0.08$ to 1.9 for $(K/N^*) = 0.14$). Little evolution is expected in our model for the EDGR brightward of $M_V \sim -16$ as the faded remnants of the dwarf irregulars do not appear brighter than this at the present day (It is not clear whether the proposed population of dwarf irregulars could metamorphose into e.g. dwarf spheroidals in the interim between $z \sim 0.2$ and the present day. The point we stress here is that with our assumption of 3 mags fading the remnants cannot affect the EDGR brightward of $M_V \sim -16$ whatever form they take). Thus from our model we expect an EDGR of $2.3_{-0.4}^{+1.0}$ in local clusters, consistent with the values observed. We conclude that there is currently no convincing evidence for strong evolution in EDGR out to $z \sim 0.2$.

Finally, turning to the “galaxy harassment” model of Moore et al. (1996) we see that the predicted evolution of the EDGR will depend critically upon the relative effect of disk stripping and central starbursts on the luminosity of the remnant dwarf spheroidal. Moore et al. suggest that the infalling field galaxies are somewhat brighter than the dIrr population in our models ($M_V \sim -19$). If the stellar luminosity lost due to stripping is less than a few times that produced by the starburst, the remnants would appear brighter than $M_V \sim -16$ in the local clusters and hence the present day EDGR would be higher than that seen at intermediate redshift, in contradiction to the observations. Clearly there is considerable scope for obtaining agreement between the harassment model and the observations, but we are encouraged by the future possibilities of closely comparing theoretical models with observations of galaxy evolution in rich clusters.

5 CONCLUSIONS

(i) We have presented deep V and I photometry of A665 and A1689, two rich, X-ray luminous clusters at $z = 0.18$. This photometry reached a limiting apparent magnitude of $I = 22.5$, equivalent to an absolute magnitude of $I = -18.0$, or $M^* + 5$, at the cluster redshifts. We analysed the data to provide differential number counts of ~ 1500 – 2000 galaxies in the fields of each of these two clusters.

(ii) We used an independent V and I field survey reaching similar depths to remove the field contamination from our cluster fields. We undertook extensive observations to calibrate the photometry between the field and cluster datasets. This gave us confidence in our field subtraction, and in the resulting cluster LF.

(iii) The LFs we derived in our two clusters also showed remarkable consistency with each other. Both showed knees, a flat region and then an upturn at the faint end (beginning around $M_V = -19$). The upturn in the cluster LFs was more marked in V than I ($\alpha \sim -2$ versus $\alpha \sim -1.2$) indicating that the faint population rapidly becomes bluer with decreasing luminosity. By means of a simple test using cumulative plots of the galaxies in each band we showed that the mean colour was $(V-I) \sim 0.6$ by $I \sim 22$ in contrast with the mean colour of the bright spheroid population, $(V-I) \sim 1.6$. Moreover, the form of the LF in our two clusters was in very good agreement with that found for a single distant cluster by Driver et al. (1994).

(iv) We constructed a simple model which described the gross features of the LFs observed in our distant clusters. The main feature of this model was the partitioning of the faint cluster component into a quiescent red dwarf elliptical population and a star forming blue dwarf irregular population. Evolving these populations forward to the present day we could fit the form of the dwarf luminosity function observed in Virgo if we assumed substantial, but not unreasonable, fading in the dIrr population.

(v) If the cessation of star formation and subsequent fading/disruption of these blue dwarf galaxies is associated with extensive gas loss from these systems, then the population seen in our distant clusters has a sufficiently steep faint end slope ($\alpha \sim -2$) to be the source of all the X-ray gas seen in local rich clusters (Trentham 1994).

(vi) Extending observational studies such as the one presented here to higher redshifts will provide further constraints on the changing form of the giant and dwarf galaxy populations in clusters, and hence the consequences for the evolution of the X-ray emission of the clusters.

ACKNOWLEDGMENTS

We are grateful to Chris Lidman for his generosity in providing and analysing the field survey, without which our analysis would have been impossible. We also thank Chris for answering all of our naive questions about his dataset. We thank Simon Driver, Neil Trentham and Ann Zabludoff for useful discussions. Many thanks are also due to Carlos Frenk for his help, support and encouragement on this project. GW gratefully acknowledges a PPARC studentship

during the time these observations were made. Support via a Carnegie Fellowship is gratefully acknowledged by IRS. IRS and RSE acknowledge support from PPARC. WJC acknowledges support from the Australian Department of Industry, Science and Technology, the Australian Research Council and Sun Microsystems. The observations described in this paper were obtained at the Isaac Newton and William Herschel Telescopes, Observatorio del Roque de los Muchachos, La Palma.

REFERENCES

- Abell G. O., 1977, *ApJ*, 213, 327
 Babul A., Ferguson H. C., 1996, *ApJ*, 458, 100
 Babul A., Rees M. J., 1992, *MNRAS*, 255, 346
 Barger A. J., Aragón-Salamanca A., Ellis R. S., Couch W. J., Smail I., Sharples R. M., 1996, *MNRAS*, 279, 1
 Bernstein G., Nichol R. C., Tyson J. A., Ulmer M. P., Wittmann D., 1996, *AJ*, 110, 1507
 Bertin E., Arnouts S., 1996, *A&AS*, 117, 393, *A&A*, submitted
 Binggeli B., Sandage A., Tammann G. A., 1985, *AJ*, 90, 1681
 Biviano A., Durret F., Gerbal D., Fevre O. L., Lobo C., Mazure A., Slezak E., 1995, *A&A*, 297, 610
 Bothun G. D., Impey C. D., Malin D. F., 1991, *ApJ*, 376, 404
 Broadhurst T. G., 1996, preprint
 Burstein D., Heiles C., 1984, *ApJS*, 54, 33
 Butcher H., Oemler A., 1984, *ApJ*, 285, 426
 Cole S., Aragón-Salamanca A., Frenk C. S., Navarro J. F., Zepf S. E., 1994, *MNRAS*, 271, 781
 Colless M. M., 1987, Ph.D. thesis, University of Cambridge
 Dressler A., 1980, *ApJ*, 236, 351
 Driver S. P., Phillips S., Davies J. I., Morgan I., Disney M. J., 1994, *MNRAS*, 268, 393 (DPDMD)
 Ellis R. S., Allington-Smith J. R., Smail I., 1991, *MNRAS*, 249, 184
 Ferguson H. C., Sandage A., 1991, *ApJ*, 101, 3
 Gudehus D. H., 1989, *ApJ*, 340, 661
 Impey C., Bothun G., Malin D., 1988, *ApJ*, 330, 634
 Kaiser N., Squires G., Fahlman G., Woods D., Broadhurst T. G., 1994, in Maddox S. J., Aragón-Salamanca A., ed, *Proc. 35th Herstmonceux conference, Wide Field Spectroscopy and The Distant Universe*. Kluwer Academic Publishers, p. 246
 Kashikawa N., Shimasaku K., Yagi M., Yasuda N., Doi M., Okamura S., Sekiguchi M., 1995, *ApJ*, 452, L99
 Landolt A. U., 1992, *AJ*, 104, L340
 Lavery R., Henry J. P., 1988, *ApJ*, 329, L21
 Lidman C. E., Peterson B. A., 1996, *MNRAS*, 279, 1357
 Lobo C., Biviano A., Durret F., Gerbal D., Fevre O. L., Mazure A., Slezak E., 1996, preprint
 Lugger P. M., 1986, *ApJ*, 303, 535
 Metcalfe N., 1983, Ph.D. thesis, University of Oxford
 Moore B., Katz N., Lake G., Dressler A., Oemler A., 1996, *Nature*, 379, 613
 Oegerle W. R., Fitchett M. J., Hill J. M., Hintzen P., 1991, *ApJ*, 376, 46
 Oemler A., 1992, in Fabian A. C., ed, *Clusters and Superclusters*, NATO ANSI series. Kluwer Academic Publishers, p. 29
 Secker J., Harris W. E., 1996, preprint
 Smail I., Dressler A., Couch W. J., Ellis R. S., Oemler A., Butcher H., Sharples R., 1996, *ApJ*
 Smail I., Hogg D. W., Yan L., Cohen J. G., 1995, *ApJ*, 449, L105
 Soltan A., Henry J. P., 1983, *ApJ*, 271, 442
 Thompson L. A., Gregory S. A., 1993, *AJ*, 106, 2197
 Trentham N., 1994, *Nature*, 372, 157

Table 1. INT cluster observations

Target	Filter	Chip	Scale ("'/pix)	Field	T _{exp} (ksec)	FWHM (")	m _{lim} (50%)	$\mu(1\sigma)$ (mag/□")	Reddening	N _{gal} ($< m_{50}$)
A665	<i>I</i>	FORD	0.37	12.34' × 12.30'	20.5	1.7	22.0	25.3	0.007	1689
A1689	<i>I</i>	EEV	0.54	11.29' × 10.61'	9.8	1.8	22.5	26.1	0.063	2035
A665	<i>V</i>	FORD	0.37	12.34' × 12.30'	17.0	2.0	23.5	26.7	0.015	1659
A1689	<i>V</i>	FORD	0.37	11.29' × 10.61'	18.0	2.1	23.5	26.9	0.098	1615

Table 2. SExtractor detection parameters

Cluster	Filter	Conv.	Min. Area (pixels)	μ_{thresh} (mag/□")
A665	<i>I</i>	3 × 3	6	24.5
A1689	<i>I</i>	3 × 3	6	25.1
A665	<i>V</i>	3 × 3	6	26.3
A1689	<i>V</i>	1 × 1	6	26.3

Turner J. A., Phillipps S., Davies J. I., Disney M. J., 1993, MN-RAS, 261, 39

Tyson J. A., Fischer P., 1995, ApJ, 446, L55

Tyson J. A., Valdes F., Wenk R., 1990, ApJ, 349, L1

Valdes F., Tyson J. A., Jarvis J. F., 1983, ApJ, 271, 431

Whitmore B. C., Gilmore D. M., Jones C., 1993, ApJ, 407, 489

This paper has been produced using the Royal Astronomical Society/Blackwell Science L^AT_EX style file.

Table 3. Schechter function parameter fits for incompleteness corrected field subtracted points. The columns show the cluster, filter, faint end slope, apparent magnitude at the knee, absolute magnitude at the knee, normalisation, χ^2 , and reduced χ^2 values. The best fit parameters found by subtracting the mean value (first row) and then the $\pm 1\sigma$ error values of background counts (second and third rows) are also shown.

Cluster	Filter	α	m^*	M^*	N^*	χ^2	χ^2/ν
A665	I	-1.065	18.11	-22.39	127.15	24.67	2.74
		-1.083	18.04	-22.46	143.03	24.54	
		-1.060	18.18	-22.32	103.57	25.41	
A1689	I	-1.321	17.42	-23.08	62.63	21.34	2.13
		-1.303	17.40	-23.10	73.40	22.40	
		-1.366	17.40	-23.10	46.76	20.54	
A665	V	-0.843	19.64	-21.18	240.54	49.36	5.49
		-0.709	19.73	-21.09	296.56	40.87	
		-1.079	19.46	-21.36	154.46	57.58	
A1689	V	-1.500	18.83	-21.99	57.25	33.33	3.70
		-1.382	19.00	-21.82	85.73	30.48	
		-1.647	18.56	-22.26	30.93	34.92	

Table 4. Schechter function parameter fits for incompleteness and obscuration corrected field subtracted points. The column headings are as in Table 3.

Cluster	Filter	α	m^*	M^*	N^*	χ^2	χ^2/ν
A665	I	-1.188	18.04	-22.46	123.00	26.03	2.89
		-1.185	17.98	-22.52	139.02	25.87	
		-1.222	18.04	-22.46	95.77	26.69	
A1689	I	-1.430	17.30	-23.20	57.04	22.12	2.12
		-1.406	17.28	-23.22	66.52	23.01	
		-1.466	17.37	-23.13	47.38	21.42	
A665	V	-1.167	19.37	-21.45	178.36	59.17	6.57
		-1.042	19.43	-21.39	233.79	52.01	
		-1.370	19.00	-21.82	96.92	64.57	
A1689	V	-1.607	18.68	-22.14	51.40	35.96	4.00
		-1.514	18.84	-21.98	74.56	34.07	
		-1.715	18.48	-22.34	31.70	36.80	

Table 5. Schechter function parameter fits for incompleteness and obscuration corrected radial inner/outer test points. The column headings are as in Table 3.

Cluster	Filter	α	m^*	M^*	N^*	χ^2	χ^2/ν
A665	I	-1.235	17.49	-23.01	40.96	1.27	0.14
A1689	I	-1.034	17.43	-23.07	139.84	10.24	1.02
A665	V	-1.264	18.82	-22.00	58.07	4.42	0.49
A1689	V	-1.681	18.09	-22.73	19.10	5.67	0.63

Table 6. Gaussian+Schechter function parameter fits. The top table gives the fits for the incompleteness and obscuration corrected catalogues, while the lower is for the incompleteness corrected case only. The columns show the cluster, filter, apparent magnitude at the peak of Gaussian function, absolute magnitude at the peak of Gaussian function, normalisation of Schechter function, faint end slope of Schechter function, apparent magnitude at the knee of Schechter function, absolute magnitude at the knee of Schechter function, χ^2 , and reduced χ^2 values. Note that σ , the standard deviation of the Gaussian function is held constant at 1.0 and K , the normalisation of the Gaussian function is required to equal $0.1 \times N^*$.

Cluster	Filter	m^{cent}	M^{cent}	N^*	α	m^*	M^*	χ^2	χ^2/ν
A665	<i>I</i>	18.36	-22.14	312.21	-0.991	20.01	-20.49	12.01	2.00
A1689	<i>I</i>	18.44	-22.06	319.99	-1.180	20.03	-20.47	11.89	1.49
Combined	<i>I</i>	18.66	-21.84	343.98	-1.160	20.23	-20.27	12.32	1.76
A665	<i>V</i>	20.55	-20.27	823.73	-2.295	22.69	-18.13	9.51	1.36
A1689	<i>V</i>	20.63	-20.19	689.95	-1.870	22.32	-18.50	9.99	1.43
Combined	<i>V</i>	20.62	-20.20	776.95	-2.092	22.55	-18.27	14.68	2.10
Cluster	Filter	m^{cent}	M^{cent}	N^*	α	m^*	M^*	χ^2	χ^2/ν
A665	<i>I</i>	18.22	-22.28	268.05	-0.841	19.97	-20.53	11.68	1.95
A1689	<i>I</i>	18.42	-22.08	290.07	-1.025	20.18	-20.32	12.01	1.50
Combined	<i>I</i>	18.64	-21.86	309.18	-1.017	20.36	-20.23	12.31	1.76
A665	<i>V</i>	20.48	-20.34	673.15	-2.464	22.81	-18.01	9.17	1.31
A1689	<i>V</i>	20.60	-20.22	572.42	-1.956	22.45	-18.37	8.92	1.27
Combined	<i>V</i>	20.56	-20.26	635.45	-2.230	22.66	-18.16	12.69	1.81